

Pentacene multilayers on Ag(111) surface

Ersen Mete,^{*,†} İlker Demiroğlu,[‡] M. Fatih Danişman,[‡] and Şinasi Ellialtıoğlu[¶]

Department of Physics, Balıkesir University, Balıkesir 10145, Turkey, Department of Chemistry, Middle East Technical University, Ankara 06531, Turkey, and Department of Physics, Middle East Technical University, Ankara 06531, Turkey

E-mail: emete@balikesir.edu.tr

Phone: +90 (0)266 6121000. Fax: +90 (0)266 6121215

*To whom correspondence should be addressed

[†]Department of Physics, Balıkesir University, Balıkesir 10145, Turkey

[‡]Department of Chemistry, Middle East Technical University, Ankara 06531, Turkey

[¶]Department of Physics, Middle East Technical University, Ankara 06531, Turkey

Abstract

The structural profiles and electronic properties of pentacene ($C_{22}H_{14}$) multilayers on Ag(111) surface has been studied within the density functional theory (DFT) framework. We have performed first-principle total energy calculations based on the projector augmented wave (PAW) method to investigate the initial growth patterns of pentacene (Pn) on Ag(111) surface. In its bulk phase, pentacene crystallizes with a triclinic symmetry while a thin film phase having an orthorhombic unit cell is energetically less favorable by 0.12 eV/cell. Pentacene prefers to stay planar on Ag(111) surface and aligns perfectly along silver rows without any molecular deformation at a height of 3.9 Å. At one monolayer (ML) coverage the separation between the molecular layer and the surface plane extends to 4.1 Å due to intermolecular interactions weakening surface–pentacene attraction. While the first ML remains flat, the molecules on a second full pentacene layer deposited on the surface rearrange so that they become skewed with respect to each other. This adsorption mode is energetically more preferable than the one for which the molecules form a flat pentacene layer by an energy difference similar to that obtained for bulk and thin film phases. Moreover, as new layers added, pentacenes assemble to maintain this tilting for 3 and 4 ML similar to its bulk phase while the contact layer always remains planar. Therefore, our calculations indicate bulk-like initial stages for the growth pattern.

Introduction

Due to its use in thin film transistor (TFT) applications pentacene is continuing to enjoy being the subject of extensive research. Since most TFT's employ SiO_2 as the dielectric layer, initial studies on pentacene focused mainly on gaining a thorough understanding of structural¹⁻⁴ and electronic⁵⁻⁸ properties of thin films of this molecule on SiO_2 surfaces and in turn achieving the best device performance by optimizing⁹⁻¹¹ these properties. As a result of this heavy research effort in the last decade, fabricating pentacene TFT's with hole mobilities of more than $1 \text{ cm}^2/\text{Vs}$ have become an almost routine process.¹² Nevertheless there are still, fundamental issues to be resolved such as the dependence of the charge mobility on the film thickness¹³ and areas open to improvement like modification of the substrate surfaces with buffer layers⁷ or the pentacene itself with functional groups.^{7,14}

Another very critical but relatively less well understood subject is the growth mechanism of pentacene films on metal substrates. Understanding the pentacene film growth on gold and silver surfaces is particularly important since these metals constitute the electrode material in most TFT's and the device performance is directly related to the charge transfer efficiency between the electrodes and the organic film. Though both experimental¹⁵⁻²⁹ and theoretical^{29,31,32} research in this field has been recently intensified, there are contradictory results in the literature and the growth modes of pentacene thin films on Au(111) and Ag(111) surfaces are continuing to be a matter of debate. This is mostly due to the relatively strong (when compared with SiO_2) interaction of the metal surfaces with the pentacene molecule. As a result of this strong interaction pentacene adopts many different monolayer and multilayer phases on metal surfaces which are energetically and structurally very close to each other. For example on Au(111) several different low density monolayer phases and an identical full coverage phase have been reported by different groups.^{15-18,20} However, in case of the multilayers while Kang et al.^{15,16} report a layer by layer growth of lying down pentacene molecules, Beernink et al.¹⁹ report strong dewetting starting from the second layer and growth of bulk like pentacene crystals. For pentacene films on Ag(111) surfaces, while Eremtchenko et al.²⁴ and Dougherty et al.²⁶ report a bilayer film formation, where an ordered

(second) layer (which follows the symmetry of the Ag(111) surface) forms on top of a disordered (2D gas phase) first layer at room temperature, Käfer et al.²¹ report the formation of bulk-like pentacene structures immediately after the first monolayer. So on both surfaces the growth mechanism of pentacene films is still not completely clear. In addition, if the above mentioned 2D gas phase mechanism for Ag(111) is really correct then questions like “Why does pentacene behave completely differently on seemingly similar surfaces, Ag(111) and Au(111)?” and “How does the symmetry of the substrate affect the bilayer film structure?” arise.

In spite of this richness of experimental studies and points in need of clarification, pentacene films on Ag(111) or Au(111) surfaces have not, yet, been studied theoretically. Theoretical work regarding pentacene films were mostly performed on other metal surfaces, such as Cu(001),³³ Cu(110),³⁴ Ag(110),²⁹ at semi-empiric level and Al(100),³⁵ Cu(100),³⁶ Cu(119),³⁷ Fe(100),³⁸ Au(001)^{31,32} at DFT level. These studies in general addressed two points concerning the first layer of pentacene film/molecule: (1) Determination of the most stable adsorption site/geometry, and (2) determination of the strength of electronic interaction/coupling between the substrate and the molecule. In these studies either the most stable configuration was found to be pentacene lying flat on the surface²⁹ or the calculations were started with this assumption. In terms of the electronic interactions, the DFT studies performed using GGA functionals found considerable aromatic- π -system metal substrate interaction^{36,37} on Cu surfaces, hinting at chemisorption. On Au(111)³² and Al(100)³⁵ however, while LDA functionals resulted in strong interactions, in the form of broadening and splitting of π -molecular orbitals, GGA functionals are reported to result in much weaker interactions, in accord with a physisorption mechanism. Theoretical studies concerning the further stages of pentacene film growth on metal surfaces, however, like second layer structure/energetics or the thin film crystal/electronic structure, are very few and at semi-empiric level.³³ Instead, theoretical works regarding pentacene films are primarily focused on the electronic structure of different pentacene polymorphs observed mainly on SiO₂ surfaces, one being the famous “thin film phase”.^{8,39–42}

Hence, a theoretical study of growth mechanism and electronic properties of pentacene films

on Ag(111) and Au(111) may, (1) help resolve the experimental contradictions mentioned above and (2) fill a gap in the theoretical literature and enable a comparison of these systems with other pentacene films. As a first attempt to this end, here we present the results of our work on the structural and electronic properties of monolayer and multilayer films of pentacene on Ag(111) at DFT level. First we discuss full coverage monolayer film in the light of experimental results. We compare the adsorption geometries and the corresponding density of states we found with the experimental results reported so far. Then we present our results regarding two and three monolayers of pentacene film and discuss how the crystal and electronic structure of the Ag(111)/pentacene interface and the film evolves with coverage. We conclude with an overall summary and discussion of the results.

Method

We performed total energy density functional theory (DFT) calculations using the projector-augmented wave (PAW) method^{43,44} within the generalized gradient approximation (GGA) by employing the Perdew–Burke–Ernzerhoff (PBE)⁴⁵ exchange–correlation energy functional as implemented in the Vienna Ab Initio Simulation Package (VASP).⁴⁶

For consistency, we used a kinetic energy cutoff of 370 eV for the plane wave expansion of single particle wavefunctions in all the calculations. Electronic ground states has been determined by requiring a total-energy convergence up to a tolerance value smaller than 0.1 meV. We used a conjugate-gradient algorithm, in all geometry optimization calculations, based on the reduction in the Hellman–Feynman forces on each constituent atom to less than 10 meV/Å.

We examined two previously known polymorphs of Pn lattice: the bulk⁴⁷ and the thin film³⁹ phases. Bulk phase corresponds to a triclinic unit cell which contains two $C_{22}H_{14}$ formulae with a set of parameters: $a = 7.90 \text{ \AA}$, $b = 6.06 \text{ \AA}$, $c = 16.01 \text{ \AA}$, $\alpha = 101.9^\circ$, $\beta = 112.6^\circ$, and $\gamma = 85.8^\circ$.⁴⁷ Our calculated values of $a = 7.90 \text{ \AA}$, $b = 6.06 \text{ \AA}$, $c = 16.01 \text{ \AA}$, $\alpha = 102.0^\circ$, $\beta = 112.6^\circ$, and $\gamma = 85.5^\circ$ shows a very good agreement with the experimental results of Campbell *et al.* For the

thin film phase, we obtained an orthorhombic unit cell with $a = 7.42 \text{ \AA}$, $b = 5.87 \text{ \AA}$, and $c = 16.21 \text{ \AA}$. These parameters agree with Parisse *et al.*'s³⁹ theoretical results of $a = 7.60 \text{ \AA}$, $b = 5.90 \text{ \AA}$, and $c = 15.43 \text{ \AA}$ except for the last one, corresponding to the longitudinal size of the unit cell. We calculated the length of an isolated molecule to be 14.5 \AA . Therefore, the disagreement, in this phase, stems from the Pn–Pn separation in the multilayers.

In order to compare the predictions of different DFT functionals with the experimental results for key structural and electronic parameters like the lattice constants and binding energies, we repeated our calculations using PW91⁴⁸ parametrization within both generalized gradient and local density approximations (LDA). We calculated the lattice parameter of the silver *ccp* bulk structure in $Fm\bar{3}m$ symmetry group to be 4.00 , 4.15 , and 4.17 \AA using LDA-PW91, GGA-PW91, and GGA-PBE functionals respectively. These compare well with the experimental⁴⁹ value of 4.09 \AA , slightly better than the previous theoretical⁵⁰ result of 4.20 \AA . The Ag(111) surface has been modeled in a four-layer slab geometry separated from their periodic images by $\sim 15 \text{ \AA}$ of a vacuum space and $3 \times 6 \times 1$ grid for the cases of 1ML to 4ML deposition, whereas in the cases of isolated Pn adsorption a larger cell is needed and therefore a three-layer-slab geometry for the Ag(111) surface and $1 \times 2 \times 1$ grid was used. For this metallic system, the number of layers has been found to be sufficiently large to represent the Ag(111) surface structure such that the geometry optimization calculations do not disturb the subsurface layer atoms from their bulk lattice positions.

Results and Discussion

Single isolated pentacene on Ag(111)

In order to study the formation of ordered Pn layers on Ag(111) we first considered a single Pn on the surface. Isolation of the molecules was achieved by using a 8×5 silver surface unit cell which sets 9.5 \AA tip-to-tip and 7.9 \AA side-to-side separations between the periodic images. We determined the minimum energy Pn/Ag(111) geometry by investigating all possible adsorption sites with a number of orientations, compatible with the lattice symmetry, at each site as shown in

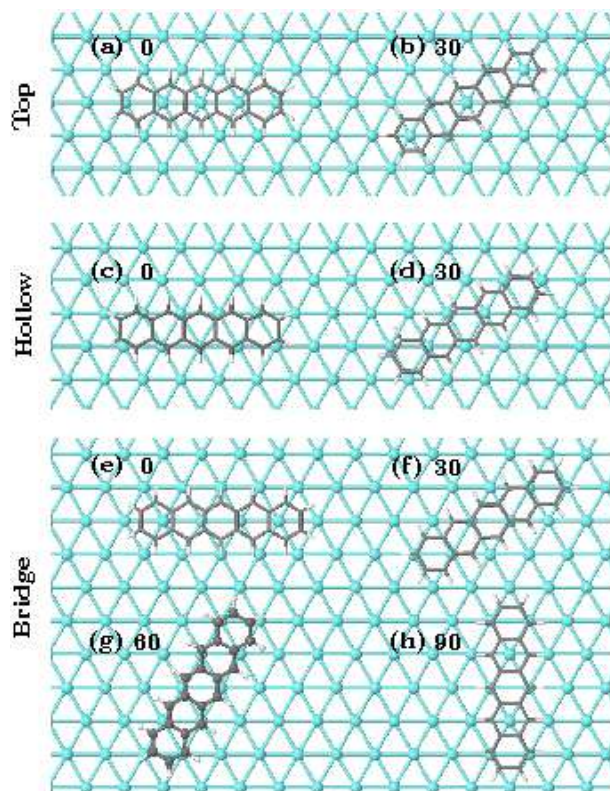


Figure 1: Single isolated pentacene on different adsorption sites of Ag(111) surface. Planar Pn adsorption with the central carbon ring on top of a silver atom aligning parallel to one of the lattice directions is abbreviated as “Top-0” (a). Top-30 in (b) refers to the adsorption at the top site with Pn major axis making an angle of 30° with any of the silver rows. Hollow-0 (c) and Hollow-30 (d) follow the same molecular alignments as the top cases, but centered on a triangle whose corners defined by Ag atoms, i.e. at the hollow site. Bridge-0 (e), Bridge-30 (f), Bridge-60 (g), and Bridge-90 (h), describe the cases where central ring of Pn lies over an Ag–Ag bond making the referred angles with any of the lattice lines. The minimum energy geometry, Bridge-60 (g), is depicted in ball-and-stick fashion while the others are all shown in sticks only.

[figure][1][1]. (Labeling conventions are described in figure caption.) In addition to these planar cases we also investigated the possibility of standing-up adsorption configurations which appeared to be around 0.15 eV less favorable than the planar ones. In geometry optimization calculations Pn develops a weak interaction with Ag(111) wherever it is initially placed on the surface. In fact, as presented in [table][1][1], the comparison of the total energies of these adsorption cases show differences which are no greater than 36 meV from each other. The flatness of the potential energy surface (PES) is indicated by the existence of such small barriers which might make Pn diffusion over the surface possible in agreement with the experimental observations that the contact layer Pn molecules are mobile at the Pn/Ag(111) interface.^{24,26} Similarly, during image acquisition STM tip has been observed to drag Pn molecules which are physisorbed on Au(111).⁵¹

Table 1: Calculated values for geometrical and electronic structure of Pn/Ag(111) systems shown in [figure][1][1]. The lateral height of isolated Pn molecule from the Ag(111) surface d_z in Å, the binding energy E_b and the relative total energy E_T in eV.

	d_z	E_b	E_T
Top-0	3.90	-0.125	0.030
Top-30	3.89	-0.119	0.036
Hollow-0	3.88	-0.147	0.008
Hollow-30	3.87	-0.128	0.027
Bridge-0	3.87	-0.124	0.031
Bridge-30	3.88	-0.124	0.031
Bridge-60	3.87	-0.155	0.000
Bridge-90	3.88	-0.129	0.026

The adsorption configurations (in [figure][1][1]) where the isolated pentacene follows the lattice symmetry so that the molecular charge density matches better with the surface charge density of silver rows are energetically more preferable. As a result, the total energy of the bridge-60 is smaller from that of the hollow-0 by only 8 meV. This also indicates that the flatness of the PES is relatively more pronounced along the lattice directions.

Single isolated pentacene molecule finds its minimum energy configuration at the bridge-60 position as depicted in ball-and-stick form in [figure][1][1]g. For this adsorption geometry, it is almost flat with a negligible bending at a height of 3.87 Å which gives a weak binding energy

of -0.155 eV. In geometry optimization calculations, for all possible initial adsorption configurations, both GGA functionals predict a weak interaction between the Pn molecule and the Ag(111) surface where LDA overbinds. (see [table][2][2]). In particular, GGA-PBE predicts that an isolated pentacene with a tilt about 15 degrees off the surface plane is only 3 meV unfavorable than the lowest energy flat geometry. This barrier is so small that the tilted pentacene does not relax back to planar geometry.

Although GGA functionals result in a weak pentacene–silver interaction, the degree of this weakness is overestimated. Since, pure DFT results depend on the choice of the exchange–correlation functional, a hybrid-DFT with corrected exchange with dispersive interaction energy would give an improved description of the binding characteristics of such a weakly bound system.⁵²

Table 2: Calculated values for electronic and geometrical structure of Ag and Pn/Ag(111) systems in different exchange–correlation functionals. Lattice parameter of Ag(111) slab a_{Ag} in Å, lateral heights d_z (Å) and the binding energies E_b (eV) of isolated and 1 ML Pn on the Ag(111) surface.

	clean slab	isolated Pn		1 ML Pn	
	a_{Ag}	d_z	E_b	d_z	E_b
LDA-PW91	4.000	2.46	-1.925	2.48	-1.753
GGA-PW91	4.145	3.69	-0.234	3.94	-0.093
GGA-PBE	4.174	3.87	-0.155	4.12	-0.078

Full monolayer

Full monolayer has been derived from the previously optimized bridge-60 configuration using an experimentally observed 6×3 silver surface unit cell.^{22,23,26} The relaxed geometry of this contact layer is shown in [figure][3][3a–c]. The molecules follow the surface symmetry and are aligned parallel to the silver rows. The distance between Pn and Ag(111) at the interface varies with varying intermolecular interaction strengths. For instance, in the case of GGA-PBE, an isolated Pn stays 3.9 Å above the surface while this value extends to 4.1 Å in the case of 1 ML coverage as presented in [table][2][2]. Corresponding binding energy at 1ML is calculated to be 0.08 eV

for GGA-PBE. This shows a weak binding similar to the experimental observations.^{22–24,26} GGA-PW91 gives a slightly better description of both the Ag substrate and Pn contact layer geometries relative to GGA-PBE results. We also calculated the supercell total energies as a function of Pn–Ag(111) distance as shown in [figure][2][2] for isolated and full monolayer cases. LDA incorrectly gives strong binding for this system since the charge densities are well localized around atoms leaving nearly empty interatomic regions.

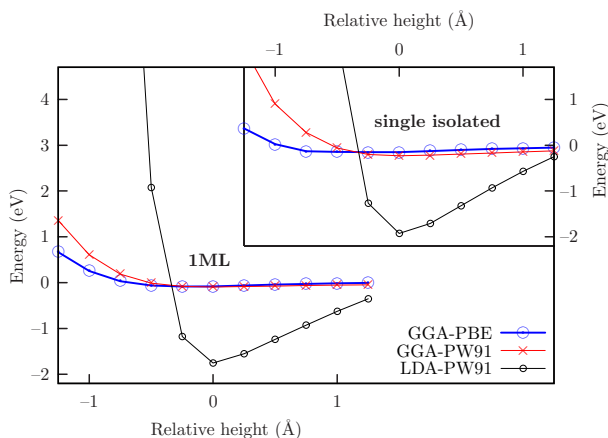


Figure 2: Binding energy versus pentacene height on Ag(111) relative to the minimum energy position (bridge-60), calculated with different exchange–correlation functionals and approximations both for a single isolated Pn and for 1ML Pn coverage.

Our DFT calculations show that a small tilt angle of the contact layer will not yield a significant increase in the total energy with respect to flat geometry. This is due to the overestimated weakness of pentacene–silver interaction. Based on these DFT results we can not reject the possibility of an average tilt at the 1ML as well as the isolated single pentacene case depending on the experimental conditions. However, our calculations do not suggest a strong binding between the pentacene layer and the surface. Therefore, our calculations indicate a flat 1 ML physisorption rather than a tilted chemisorbed Pn layer which was concluded by Käfer *et al.*²¹ based on their NEXAFS and thermal desorption signatures.

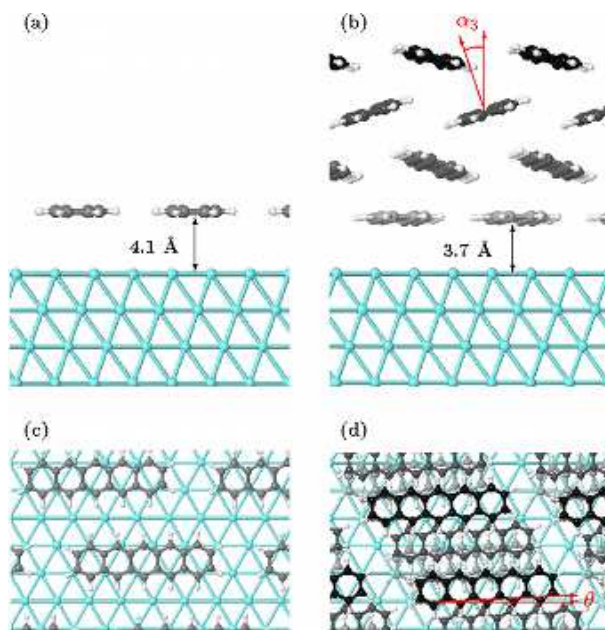


Figure 3: Side views (a, b) and top views (c, d) of (1ML, 4ML) pentacene, respectively, adsorbed on the Ag(111) surface. No perspective depth is used in the production of the figures, hence the actual tilts are seen in (b) and (d) for the 4ML case.

Multilayers

We considered two different initial geometries for the second pentacene layer on the already optimized 1ML Pn/Ag(111) structure. For the first case, the second layer molecules are flat on the first monolayer where molecular axes follow the surface symmetry. In addition, a second layer pentacene stays above in between the two molecules underneath. The second case initial structure is the same as the first one except the molecular planes of only the second layer pentacenes are tilted around their long axes as observed in experimental studies.^{21–24,26} Geometry optimization calculations resulted in a very small difference of 0.046 eV in the total energies in favor of the latter case in which second layer molecules slightly misaligned from the surface lattice direction by 6.4° in addition to the molecular plane tilting of 18° as presented in [table][3][3]. The smallness of the energy difference between the two cases can be addressed to the energy difference between the different phases of pentacene. For instance, we calculated the difference in the total energies between the bulk and the thin film phases of pentacene to be 0.12 eV for a cell having two molecular formulae units.

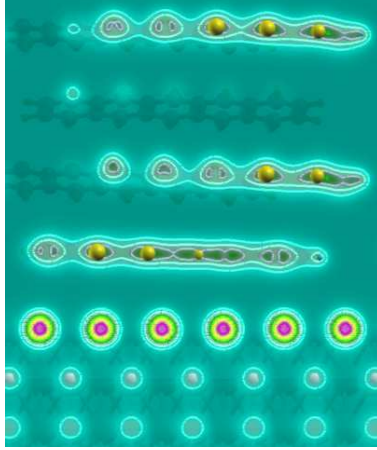


Figure 4: The charge density contour plot of 4 ML pentacene–Ag(111) interface on a plane normal to the surface and cut through a silver row.

For the 2ML structure, the tilted layer (the second one) relaxes to a height of 3.6 Å above the contact layer which is separated from the silver surface by 3.8 Å. Resulting height of the first tilted pentacene layer from silver surface becomes 7.4 Å. In the case of 3ML and 4ML structures this height converges to 7.2 Å which is slightly lower than the experimental value of 7.8 Å reported by Danisman *et al.*.

Table 3: Calculated values for geometrical structure of Pn/Ag(111) systems where d_z is the distance between first-layer pentacene and Ag(111) surface, d_{n-m} is the distance between n th and m th Pn layers (all in Å). θ and α_n are the tilt angles of the n th layer molecules about the (111)-axis and about their major axes, respectively.

	d_z	d_{1-2}	d_{2-3}	d_{3-4}	θ	α_2	α_3	α_4
isolated	3.9	–	–	–	0.0	–	–	–
1ML	4.1	–	–	–	0.0	–	–	–
2ML	3.8	3.6	–	–	6.4	18	–	–
3ML	3.7	3.5	3.6	–	6.0	25	–17	–
4ML	3.7	3.5	3.5	3.6	4.0	20	–23	15

The flat and tilted pentacene configurations above the first layer has also been considered for the 3ML and 4ML initial structures. The difference in the total energies has been calculated to be 0.127 eV and 0.125 eV in favor of the tilted molecules on the first layer for 3ML and 4ML cases, respectively. Therefore, bulk-like pentacene formation on Ag(111) surface above the contact layer is more preferable than flat lying multilayers.

In the case of multilayers, the separation of the top layer from the layer underneath is 3.6 Å and all the inner interlayer distances become 3.5 Å while the height of the contact layer converges to a value of 3.7 Å after the third ML. In addition, our calculations show a decrease in the misalignment of pentacenes above the contact layer as new layers deposited on Ag(111) surface up to 4ML. All multilayer geometries can be seen through [figure][3][3b–d, which only show views of the 4ML structure, since the interlayer distances and angles do not change significantly as new layers added. We also present the corresponding electronic density contour plot of pentacene–Ag(111) interface at 4ML in [figure][4][4 which indicates charge localization around pentacene molecules and in the substrate suggesting weak binding of the contact layer.

Consequently, the thin film formation starting from the second ML indicates that the intermolecular interactions are relatively stronger than the pentacene–silver interaction. Substantiated, the misalignment of pentacenes above the contact layer can also be attributed to the weakness of Pn–Ag(111) interaction. In fact, this observation is in parallel with the experimental observations of Danisman et al.⁵³ whereupon desorption of the pentacene multilayers on a stepped Ag(111) surface a new monolayer phase was observed. In addition, tilted second layer structure was also reported by both Eremthcenko et al.²⁴ and Käfer et al.²¹ Furthermore, molecular rearrangements involving such topological phase transformations from flat to buckled pentacene multilayers mimicking thin film formation on Ag(111) can be expected to give the same order of energy differences as that of thin film and the bulk pentacene phases. One final point to be stressed here is that, although (i) our results may be helpful for the comparison of stability of flat and tilted multilayers, and (ii) the more stable multilayer configurations we found resemble the experimentally observed pentacene phases^{21–23,41,47} (i.e., the tilt angles are very close to that of pentacene bulk and thin film phases), a direct comparison of our results with the experimentally observed structures may not be very meaningful. This is because the multilayer and monolayer in-plane unit-cell dimensions which are actually different had to be chosen the same due to computational restrictions.

In order to investigate the coupling of the frontier molecular orbitals of pentacene to the silver

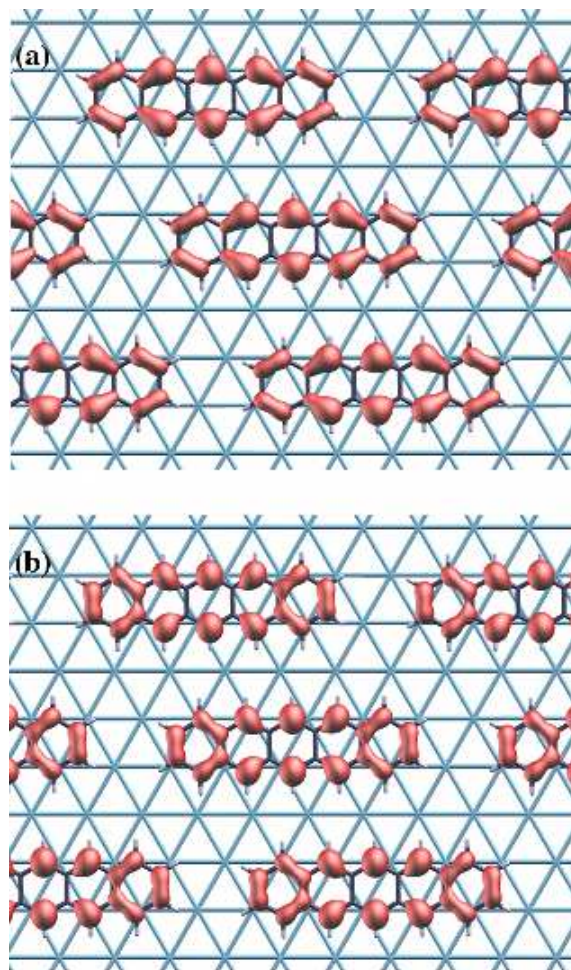


Figure 5: Calculated STM image of 1ML Pn on Ag(111) (a) for the occupied states around -0.9 eV and (b) for the unoccupied states around 1.3 eV vicinity of the Fermi energy.

substrate states, we obtained the STM pictures by using Tersoff–Hamann approximation.⁵⁴ The calculated STM images for the applied voltages of -0.9 V and 1.3 V in [figure][5][5] resemble to the HOMO and LUMO charge densities of an isolated Pn similar to Lee *et al.*'s result.³¹ Our results also agree well with the recent differential conductance images obtained with low-temperature STM experiments for seemingly similar physisorption system of pentacene/Au(111).⁵¹ These STM images in [figure][5][5] are consistent and are also apparent from the PDOS of 1ML Pn/Ag(111) presented in [figure][6][6]. The first PDOS peak of the Pn layer about 0.5 eV below the Fermi energy comes from the HOMO's of the molecules. The sharpness of this peak substantiates that the frontier orbitals of the Pn molecules mixes very weakly with the $5s$ states of the surface Ag atoms. Hence, STM calculation covering an energy range of 0.9 eV below the Fermi level shows HOMO

charge density for Pn layer over the slab as shown in [figure][5][5] where the small Ag 5s contribution was suppressed for visual convenience. Similarly, the first peak due to Pn layer about 0.7 eV above the Fermi energy corresponds to the LUMO's of the molecules which are also weakly mixing with the valence bands of Ag(111). At this point, in order to comment on the reliability of our method, we compare the experimental and theoretical results of Pn–Cu(100). Ferretti et al.,³⁶ on this system, have found a significant broadening of pentacene HOMO–LUMO bands and mixing with the substrate levels using the same computational procedure. This, in combination with the experimental results, were interpreted as an interaction close to chemisorption. In Pn–Ag(111) case, however, it is clear from our results that the picture is more close to physisorption.

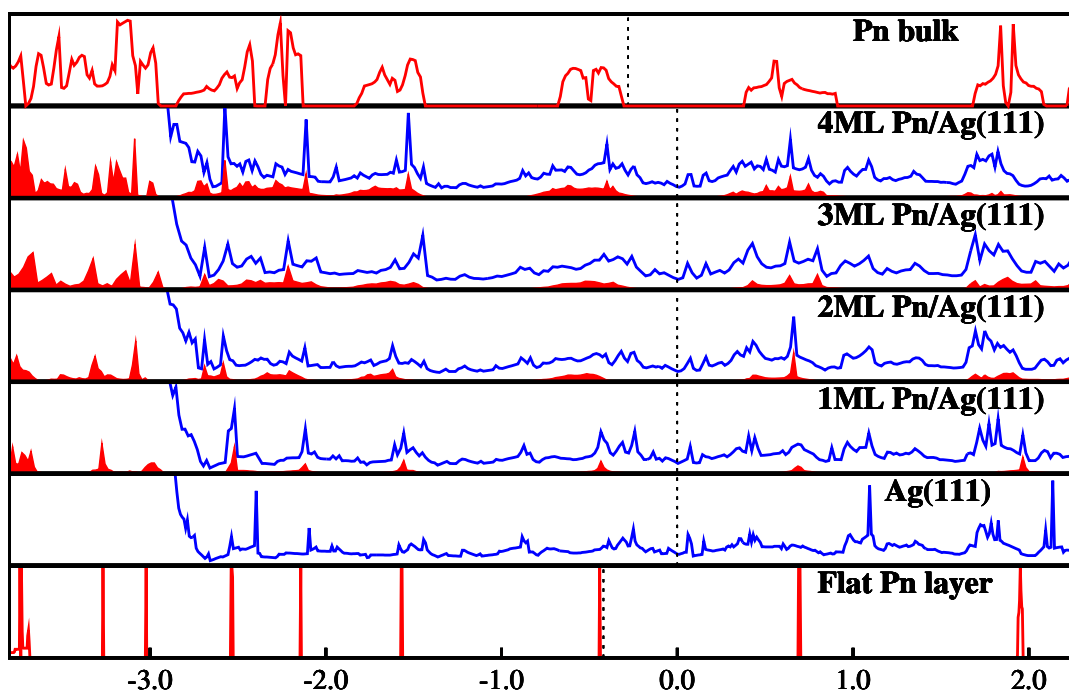


Figure 6: (color online) Calculated PDOS for Pn/Ag(111) structures. The abscissa is the energy, in eV, relative to the Fermi level for the clean Ag(111) surface. Pentacene contributions are indicated by gray (red) while total DOS is in dark gray (blue).

The bottom panel of [figure][6][6] shows the calculated DOS for the flat pentacene layer which is obtained by removing the silver substrate from 1ML/Ag(111) ([figure][3][3a–c) structure. The sharp peaks, having less structure, rather look like an energy level diagram due to very low overlap between molecular orbitals through tip to tip pentacene contacts over the layer. Metallic nature of

the bare Ag(111) surface is also presented in the succeeding panel of [figure][6][6] where Fermi level is set as the origin of the energy axis. The DOS structure corresponding to full pentacene monolayer on Ag(111) is shown in the third panel from the bottom in [figure][6][6]. DOS peaks stemming from pentacene show no shift in energy with respect to those of the flat Pn layer in the absence of the metal substrate. In addition, the broadening of each peak is localized over a small number of silver states indicating weak semiconductor–metal coupling. As a result of this weak interaction, the contact layer shows bulk-like HOMO–LUMO contributions to the total DOS around the Fermi energy. Therefore, STM experiments capture these frontier molecular orbitals.

As new pentacene layers deposited on the first full monolayer the corresponding PDOS contribution starts to form localized satellite structures at around flat Pn layer peak positions. Their broadening is larger than the broadening in PDOS peaks obtained for 1ML/Ag(111). This indicates that the interlayer molecular orbital overlap is relatively stronger than the coupling between the contact layer and the metal substrate. Moreover, these PDOS satellites match perfectly with the bulk pentacene DOS which is presented in the top panel of [figure][6][6]. Therefore, energetically preferable thin film pentacene phase on Ag(111) up to 4ML possesses bulk-like DOS properties.

Our DOS calculations show that pentacene has no electronic contribution at the Fermi energy. Evidently, highly ordered pentacene multilayers on Ag(111), considered in this study, does not exhibit band transport. In addition, these multilayers occur in bulk-like phase where the overlap of the molecular orbitals between nearest neighbor pentacenes yield large π -conjugation length along the molecular axis. Therefore, our results suggest a hopping mechanism between the localized states for the carrier transport.

Conclusion

In conclusion, we have investigated the geometric and electronic structure of pentacene on Ag(111) surface up to 4 ML coverage at the DFT level where GGA functionals perform better. At the most stable configuration a single isolated pentacene lies flat at 3.9 Å above Ag(111) surface on the

so called Bridge-60 position with a weak binding energy of -0.155 eV. For the full monolayer coverage, molecules align perfectly with the silver rows on the surface while the ML height extends slightly to 4.1 \AA due to intermolecular interactions. Calculated binding energies as well as STM and PDOS structures indicate weak pentacene–substrate coupling.

Pentacenes above the contact layer favor the thin film multilayer structure over the planar configuration with a slight energy difference which can be addressed to the small energy barriers between different phases of pentacene. Moreover, the slight misalignment of pentacene molecules above the first layer from the surface silver rows indicate that a bulk-like thin film phase starting from the second layer is adsorbed on the Ag(111) surface through a contact layer at the interface.

References

- (1) Dimitrakopoulos, C. D.; Malenfant, P. R. L. *Adv. Mater.* **2002**, *14* (2), 99–117.
- (2) Ruiz, R.; Nickel, B.; Koch, N.; Feldman, L. C.; Haglund, R. F.; Kahn, A.; Scoles, G. *Phys. Rev. B* **2003**, *67*, 125406.
- (3) Ruiz, R.; Choudhary, D.; Nickel, B.; Toccoli, T.; Chang, K. C.; Mayer, A. C.; Clancy, P.; Blakely, J. M.; Headrick, R. L.; Iannotta, S.; Malliaras, G. G. *Chem. Mater.* **2004**, *16* (23), 4497–4508.
- (4) Mattheus, C. C.; Dros, A. B.; Baas, J.; Oostergetel, G. T.; Meetsma, A.; de Boer, J. L.; Palstra, T. T. M. *Synthetic Metals* **2003**, *138* (3), 475–481.
- (5) Coropceanu, V.; Cornil, J.; da Silva, D. A.; Olivier, Y.; Silbey, R.; Bredas, J. L. *Chemical Reviews* **2007**, *107* (4), 926–952.
- (6) Fukagawa, H.; Yamane, H.; Kataoka, T.; Kera, S.; Nakamura, M.; Kudo, K.; Ueno, N. *Phys. Rev. B* **2006**, *73*, 245310.
- (7) Anthony, J. E. *Angewandte Chemie–International Edition* **2008**, *47* (3), 452–483.

- (8) Troisi, A.; Orlandi, G. *J. Phys. Chem. B* **2005**, *109* (5), 1849–1856.
- (9) Yanagisawa, H.; Tamaki, T.; Nakamura, M.; Kudo, K. *Thin Solid Films* **2004** *464-465*, 398–402.
- (10) De Angelis, F.; Toccoli, T.; Pallaoro, A.; Coppede, N.; Mariucci, L.; Fortunato, G.; Iannotta, S. *Synthetic Metals* **2004**, *146* (3), 291–295.
- (11) Locklin, J.; Roberts, M. E.; Mannsfeld, S. C. B.; Bao, Z. N. *Polymer Reviews* **2006**, *46* (1), 79–101.
- (12) Kelley, T. W.; Baude, P. F.; Gerlach, C.; Ender, D. E.; Muyres, D.; Haase, M. A.; Vogel, D. E.; Theiss, S. D. *Chem. Mater.* **2004**, *16* (23), 4413–4422.
- (13) Ruiz, R.; Papadimitratos, A.; Mayer, A. C.; Malliaras, G. G. *Adv. Mater.* **2005**, *17* (14), 1795.
- (14) Anthony, J. E. *Chem. Rev.* **2006**, *106* (12), 5028–5048.
- (15) Kang, J. H.; Zhu, X. Y. *Appl. Phys. Lett.* **2003**, *82* (19), 3248–3250.
- (16) Kang, J. H.; Zhu, X. Y. *Chem. Mater.* **2006**, *18* (5), 1318–1323.
- (17) France, C. B.; Schroeder, P. G.; Parkinson, B. A. *Nano Letters* **2002**, *2* (7), 693–696.
- (18) France, C. B.; Schroeder, P. G.; Forsythe, J. C.; Parkinson, B. A. *Langmuir* **2003**, *19* (4), 1274–1281.
- (19) Beernink, G.; Strunskus, T.; Witte, G.; Woll, C. *Appl. Phys. Lett.* **2004**, *85* (3), 398–400.
- (20) Käfer, D.; Ruppel, L.; Witte, G. *Phys. Rev. B* **2007**, *75*, 085309.
- (21) Käfer, D.; Witte, G. *Chem. Phys. Lett.* **2007**, *442* (4–6), 376–383.
- (22) Casalis, L.; Danisman, M. F.; Nickel, B.; Bracco, G.; Toccoli, T.; Iannotta, S.; Scoles, G. *Phys. Rev. Lett.* **2003**, *90*, 206101.

- (23) Danisman, M. F.; Casalis, L.; Scoles, G. *Phys. Rev. B* **2005**, *72*, 085404.
- (24) Eremtchenko, M.; Temirov, R.; Bauer, D.; Schaefer, J. A.; Tautz, F. S. *Phys. Rev. B* **2005**, *72*, 115430.
- (25) Zhang, H. L.; Chen, W.; Huang, H.; Chen, L.; Wee, A. T. S. *J. Am. Chem. Soc.* **2008**, *130* (9), 2720–2721.
- (26) Dougherty, D. B.; Jin, W.; Cullen, W. G.; Reutt-Robey, J. E.; Robey, S. W. *J. Phys. Chem. C* **2008**, *112* (51), 20334–20339.
- (27) Floreano, L.; Cossaro, A.; Cvetko, D.; Bavdek, G.; Morgante, A. *J. Phys. Chem. B* **2006**, *110* (10), 4908–4913.
- (28) Zheng, Y.; Qi, D. C.; Chandrasekhar, N.; Gao, X. Y.; Troadec, C.; Wee, A. T. S. *Langmuir* **2007**, *23* (16), 8336–8342.
- (29) Wang, Y. L.; Ji, W.; Shi, D. X.; Du, S. X.; Seidel, C.; Ma, Y. G.; Gao, H. J.; Chi, L. F.; Fuchs, H. *Phys. Rev. B* **2004**, *69*, 075408.
- (30) Pedio M.; Doyle B.; Mahne N.; Giglia A.; Borgatti F.; Nannarone S.; Henze S. K. M.; Temirov R.; Tautz F. S.; Casalis L.; Hudej R.; Danisman M. F.; Nickel B. *Adv. Surf. Sci.* **2007**, *254*, 103.
- (31) Lee, K.; Yu, J. Y. *Surf. Sci.* **2005**, *589* (1–3), 8–18.
- (32) Lee, K.; Yu, J. J.; Morikawa, Y. *Phys. Rev. B* **2007**, *75*, 045402.
- (33) Satta, M.; Iacobucci, S.; Larciprete, R. *Phys. Rev. B* **2007**, *75*, 155401.
- (34) Ample, F.; Joachim, C. *Surf. Sci.* **2006**, *600* (16), 3243–3251.
- (35) Simeoni, M.; Picozzi, S.; Delley, B. *Surf. Sci.* **2004**, *562* (1–3), 43–52.

- (36) Ferretti, A.; Baldacchini, C.; Calzolari, A.; Di Felice, R.; Ruini, A.; Molinari, E.; Betti, M. *G. Phys. Rev. Lett.* **2007**, *99*, 046802.
- (37) Baldacchini, C.; Mariani, C.; Betti, M. G.; Vobornik, I.; Fujii, J.; Annese, E.; Rossi, G.; Ferretti, A.; Calzolari, A.; Di Felice, R.; Ruini, A.; Molinari, E. *Phys. Rev. B* **2007**, *76*, 245430.
- (38) Sun, X.; Suzuki, T.; Yamauchi, Y.; Kurahashi, M.; Wang, Z. P.; Entani, S. *Surf. Sci.* **2008**, *602* (6), 1191–1198.
- (39) Parisse, P.; Ottaviano, L.; Delley, B.; Picozzi, S. *J. Phys.:Condens. Matter* **2007**, *19*, 106209.
- (40) Doi, K.; Yoshida, K.; Nakano, H.; Tachibana, A.; Tanabe, T.; Kojima, Y.; Okazaki, K. *J. Appl. Phys.* **2005**, *98*, 113709.
- (41) Nabok, D.; Puschnig, P.; Ambrosch-Draxl, C.; Werzer, O.; Resel, R.; Smilgies, D.-M. *Phys. Rev. B* **2007**, *76*, 235322.
- (42) Mattheus, C. C.; de Wijs, G. A.; de Groot, R. A.; Palstra, T. T. M. *J. Am. Chem. Soc.* **2003**, *125* (20), 6323–6330.
- (43) Blöchl, P. E. *Phys. Rev. B* **1994**, *50*, 17953.
- (44) Kresse, G.; Joubert, D. *Phys. Rev. B* **1999**, *59*, 1758.
- (45) Perdew, J. P.; Burke, K.; Ernzerhof, M. *Phys. Rev. Lett.* **1996**, *77*, 3865.
- (46) Kresse, G.; Hafner, J. *Phys. Rev. B* **1993**, *47*, 558.
- (47) Campbell, R. B.; Monteath, R. J.; Trotter, J. *Acta Crystallogr.* **1962**, *15*, 289.
- (48) Perdew, J. P.; Chevary, J. A.; Vosko, S. H.; Jackson, K. A.; Pederson, M. R.; Singh, D. J.; Fiolhais, C. *Phys. Rev. B* **1992**, *46*, 6671.
- (49) Moruzzi, V. L.; Janak, J. F.; Schwarz, K. *Phys. Rev. B* **1988**, *37*, 790.

- (50) Li, W.-X.; Stampfl, C.; Scheffler, M. *Phys. Rev. B* **2002**, *65*, 075407.
- (51) Soe, W.-H.; Manzano, C.; De Sarkar, A.; Chandrasekhar, N.; Joachim, C. *Phys. Rev. Lett.* **2009**, *102*, 176102.
- (52) Murdachaew, G.; de Gironcoli, S.; Scoles G. *J. Phys. Chem. A* **2008** *112*, 9993.
- (53) Danisman M. F.; Casalis L.; Scoles G., unpublished results.
- (54) Tersoff, J.; Hamann, D. R. *Phys. Rev. B* **1985** *31*, 805.